



HAL
open science

Experimental and micromechanical investigation on the mechanical and durability properties of recycled aggregates concrete

Ayodele Adessina, Amor Ben Fraj, Jean-François Barthélémy, Camille Chateau, Denis Garnier

► To cite this version:

Ayodele Adessina, Amor Ben Fraj, Jean-François Barthélémy, Camille Chateau, Denis Garnier. Experimental and micromechanical investigation on the mechanical and durability properties of recycled aggregates concrete. *Cement and Concrete Research*, 2019, 126, pp.105900. 10.1016/j.cemconres.2019.105900 . hal-02344042

HAL Id: hal-02344042

<https://hal.science/hal-02344042>

Submitted on 21 Dec 2021

HAL is a multi-disciplinary open access archive for the deposit and dissemination of scientific research documents, whether they are published or not. The documents may come from teaching and research institutions in France or abroad, or from public or private research centers.

L'archive ouverte pluridisciplinaire **HAL**, est destinée au dépôt et à la diffusion de documents scientifiques de niveau recherche, publiés ou non, émanant des établissements d'enseignement et de recherche français ou étrangers, des laboratoires publics ou privés.



Distributed under a Creative Commons Attribution - NonCommercial 4.0 International License

Experimental and micromechanical investigation on the mechanical and durability properties of recycled aggregates concrete

Ayodele Adessina^{a,b}, Amor Ben Fraj^a, Jean-François Barthélémy^a, Camille Chateau^b, Denis Garnier^b

^a*Cerema, Project-team DIMA, 110 Rue de Paris, BP 214, 77487, Provins Cedex France.*

^b*Laboratoire Navier, UMR 8205, CNRS, ENPC, IFSTTAR, Université Paris-Est, Marne-la-Vallée F-77455, France.*

Abstract

In this work, we conducted an experimental and micromechanical investigation on the mechanical and chloride diffusion properties of recycled aggregates concrete (RAC). Due to the composite aspect of the recycled concrete aggregates (RCA), their impact on the properties of concretes is first evaluated by conducting an experimental campaign and further numerically modeled using micromechanical tools. Local mechanical properties of phases such as the attached mortar, the interfacial transition zones (ITZ) and the aggregates are also investigated by means of indentation tests at nano and microscale. Finally, experimentally informed multi scale model is established and the overall elastic modulus and chloride diffusion coefficient of concretes (with different rates of RCA) are computed and compared to experimental results at macroscopic scale for discussion. The established model provides a predictive tool for the mechanical and chloride diffusion properties of RAC.

Keywords: Recycled aggregates concrete, elasticity, chloride diffusion, indentation, micromechanics.

1 Introduction

The increasing and unsustainable consumption of natural resources as well as the excessive production of waste from construction and demolition are an environmental and economical challenges. Indeed, as the rate of demolition is still increasing and the supply of suitable natural aggregates is rapidly dwindling due to their over-exploitation, it is essential to effectively reuse demolition waste in order to conserve natural resources. Moreover, the use of recycled aggregates (as an alternative

Email address: ayodele.adessina@cerema.fr (Ayodele Adessina)

for natural aggregates) is known to be environmentally friendly, since it decreases the delivery distance of aggregates [1].

First, most of the studies on the mechanical properties of concretes containing RCA point out the fact that, the recycled aggregate concretes exhibits weakened mechanical properties compared to the conventional concretes [2, 3, 4, 5]. Accordingly, mechanical properties such as the compressive strength, the elastic moduli and the tensile strength of recycled concretes (RAC) are found to depend on the amount of RCA in the microstructure [4], apart from other mixing parameters such the water to binder ratio. Indeed, the numerous interfacial transition zones denoted ITZ (with high level of porosity [2]) and the weakened properties of the attached mortar are known as the main factors justifying the reduced mechanical properties of the RAC. Furthermore, Padmini et al. [4], when investigating the relationship between the quality of the 'parent concrete' (from which the recycled aggregates are extracted) and the mechanical properties of the resulting RAC, show that the properties of the latter are entirely related to parameters such as the physical and mechanical properties of the parent concrete and the mixing proportions of the concrete content (water to binder ratio for instance). As for the mechanical properties of the individual phases such as the cement paste and the ITZ, nanoindentation tests are successfully conducted on this phases as reported in recent works [6, 7].

On the other hand, the durability properties of concretes are also affected by the replacement of natural aggregates by the RCA. Therefore, the chloride diffusion coefficient of RAC is found to be higher than that of the conventional concretes [2]. This aspect is explained by the high porosity of RCA leading the resulting recycled concretes to be more permeable than natural concretes with the same water to binder ratio. This argument is also used to explain the important carbonation depth measured in RAC [2, 5]. However, in a recent work, Thomas et al. [8] show that, durability properties of recycled concretes can be improved by the adjustment of the water/cement ratio since for relatively reduced water/cement ratio, the matrix (herein the mortar) is less porous and therefore compensates the high porosity of the RCA.

In the framework of micromechanical investigation of the properties of cement based materials, concretes are generally considered as three phase materials at mesoscale [9, 10, 11]. Therefore, the microstructure of the latter is assumed to be made up of matrix (mortar) embedding inclusions with interfaces (aggregates surrounded by interfacial transition zones (ITZ)) at mesoscale. Consequently, the effective properties (mechanical and durability) of concretes are derived from the available

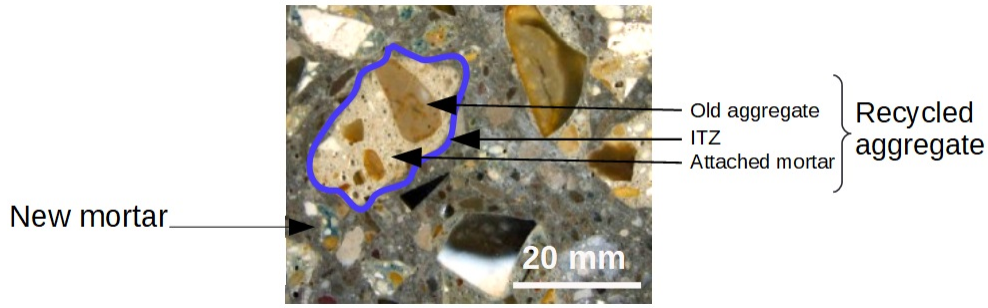


Fig. 1: Different phases in the microstructure of RAC

information on the microstructure at each specific level (volume fraction, properties of phases, size,...) [12]. The particular case of RAC introduces additional parameters to be considered. In fact, recycled aggregates are composite materials containing coarse aggregates, old and new ITZ, associated with the old or attached mortar [2, 4] (Fig.1). Although intensive works have been conducted in last decades to understand and to predict the properties of RAC, questions still arise about how does the microstructure of RAC influences the observed macroscopic behavior.

This work seeks to investigate, at different scales, the properties of high-performance recycled aggregate concretes, in order to establish a predictive micromechanical model for macroscopic effective properties. For this purpose, the adopted procedure is organized into three parts :

- The first part is devoted to the quantification of the impact of a progressive replacement of NA by RCA, on the mechanical and durability properties of RAC. In this part, specimen of recycled concretes are fabricated, submitted to mechanical and durability tests (compressive strength, elastic moduli, carbonation, chloride migration) and the results are presented for discussion.
- The second part deals with the relationship between the macroscopic behavior of RAC and the microstructural properties of individual phases (aggregates, interfacial transition zones, attached mortar). For this purpose, local mechanical properties of the phases (hardness, elastic modulus, volume fractions and distribution) are characterized using indentation tests at nano and micro scale, combined with optical and Atomic Force Microscopy observations .
- The third part addresses the modeling of the macroscopic behavior of RAC using multi scale approach. Results collected on the microstructure of the RAC (in section 3) are used as input information for the micromechanical based models. Effective elastic modulus and chloride diffusion coefficient are predicted for different replacement rates and the results are compared to those obtained at macroscopic scale (in section 2). The purpose of this part is to establish predictive models efficient to estimate the macroscopic behavior of RAC.

The paper is organized as follow : the section 2 is devoted to the experimental campaign at macroscopic scale (method, material, tests and results) whereas section 3 deals with the characterization of the microstructure (the indentation test at nano and microscale for different phases (aggregates, attached mortar, ITZ)). Finally, section 4 and 5 present the modeling of the elastic modulus and the chloride diffusion problem of RAC with different volume fractions of RCA. Results of the models are compared to experimental data for discussion.

2 Experimental study of the mechanical and durability properties of recycled aggregates concrete

2.1 Materials

For the preparation of the concretes, ordinary portland cement (CEM I 52.5N PM ES) from Leteil plant is used for the study. The natural aggregates are calcareous aggregates (grading 4/20 mm) associated with the fine aggregates (sand 0/4 mm). The recycled aggregates used in the experimental campaign are extracted from the demolishing process of a pile [1] and are classified as aggregates of type 1 according to the standard NF EN 933 – 1 [13]. The physical and mechanical properties of the aggregates are resumed in Table 1. The parent concrete (from which the recycled

Aggregates	Natural aggregates		Recycled aggregates	
Grading(mm)	4/12	12/20	4/10	10/20
Unit weight (g/cm ³)	2.65	2.72	2.26	2.5
Water absorption(%)	0.7	0.6	5.3	5.5
LA	23	22	32	35
MDE	16	11	36	27

TABLE 1: Physical and mechanical properties of the aggregates of interest (according to the standards NF EN 1097 – 1, 2, 6 [14, 15]). LA : Los Angeles coefficient, MDE : Micro Deval coefficient

aggregates are extracted) is made with a CEM III 52.5L cement with a water/cement ratio of 0.43

and characterized by a compressive strength and elastic modulus of respectively 50.5 ± 1 MPa and 51 ± 1 GPa at 90 days (measured in laboratory on reconstructed concrete).

2.2 *Mix proportion*

Due to the high water absorption of the RCAs, and in order to avoid any disturbance in the hydration process, the recycled coarse aggregates were presoaked 24 hours before mixing. Consequently, when substituting the natural aggregates by the recycled ones, some adjustments in concrete dosage are necessary as regards the volume compensation and presoaking water for recycled aggregates. Therefore, the necessary volume of water is calculated by taking into account the water absorption coefficient of the RCAs and the volume of super-plasticizer as reported in Table(1). The targeted concretes are high performance concretes made with recycled aggregates with a good workability (160–210 mm). The water / cement ratio was set to 0.42 for all the different formulas of concretes. The changing parameter was the replacement rate of natural aggregates by recycled ones. For the sake of simplicity, we adopted the notation C[replacement rate] for different formulas of concretes. Apart from the natural concrete C[0] (without recycled aggregates), five other formulas of concretes were fabricated corresponding to 20, 40, 60, 80 and 100% of replacement rate in volume. The mixing proportions are summarized in Table 2.

2.3 *Preparation of the specimens*

The preparation of all the mixes was conducted with concrete mixer of 80 litres. The sand, the cement, and the coarse aggregates were placed and dry mixed for about 2 min before water was added. After 5 min of mixing, the slump test was run in order to determine the workability of the obtained concrete (Table(3)). Thereafter, the mixture was casted in cylindrical specimens 110 mm \times 220 mm and vibrated. Finally, the specimens were demoulded after 24 hours and were cured in water at 20° C until the different testing days (at 28 and 90 days).

2.4 *Tests and results*

The following section presents the results of the tests conducted on the concretes with different replacement rates of RCA at fresh and hardened states. It helps to quantify the impact of the RCA on the mechanical and durability properties of RC.

Mixture	C[0]	C[20]	C[40]	C[60]	C[80]	C[100]
Replacement rate (%)	0	20	40	60	80	100
Cement	380					
Sand	867.8					
NA (4-12mm)	432	345.6	259.20	172.80	86.40	0
RCA (4-12mm)	0	77.02	154.03	231.05	308.52	385.08
NA (12-20mm)	561.2	448.96	336.72	224.48	112.24	0
RCA (12-20mm)	0	99.63	199.26	298.89	398.52	498.14
Effective water/cement ratio	0.42					
Super-plasticizer	2					

TABLE 2: Mix proportion of the concrete (kg/m^3). NA : Natural aggregates. The super plasticizer used is the Master Glenium 671.

2.4.1 Workability and density

The slump of the fresh concrete is measured according to the standard NF EN 12350 – 2 [16]. The slump test was carried out on two batches of 40 litres each for the different concretes and the resulting value of slump emerges from the average over the two mixtures. According to the results (Table(3)), the obtained slumps are in the range 160 – 210 mm which corresponds to the slumps of the targeted S4 class [16]. The relatively weak variation of the slumps with different replacement rates is related to the difference of the water absorption between presoaked RCA and NA. On the other hand, additional test was conducted on the aggregates in order to evaluate the density of the fabricated concretes at fresh and hardened states. The results shown in Table(3) reveal logically

Formulas	C[0]	C[20]	C[40]	C[60]	C[80]	C[100]
Slump(mm)	200±0	210±7	210±14.1	200±7.0	190±7.1	180±14.1
Density (Fresh state)	2.6	2.56	2.54	2.53	2.48	2.46
Density (Hardened state)	2.56	2.55	2.53	2.52	2.47	2.44

TABLE 3: Physical properties of the studied concretes. Density (g/cm^3).

the decrease of the concrete density with increasing volume of RCA. This reflects the impact of the density of the recycled aggregates on that of RCs especially when their volume fractions increases.

2.4.2 Compressive strength and elastic modulus

On the test days (28 and 90 days), the specimens were removed from water and their surfaces get prepared (in order to obtain perfectly smooth and parallel surfaces). Thus, tests are conducted according to the standards NF EN 12390 – 3 [17], NF EN 12390 – 13 [18] in order to evaluate, respectively, the compressive strength and the elastic modulus of concretes with different replacement rates. For each formula, the results are obtained by averaging results of at least three tests.

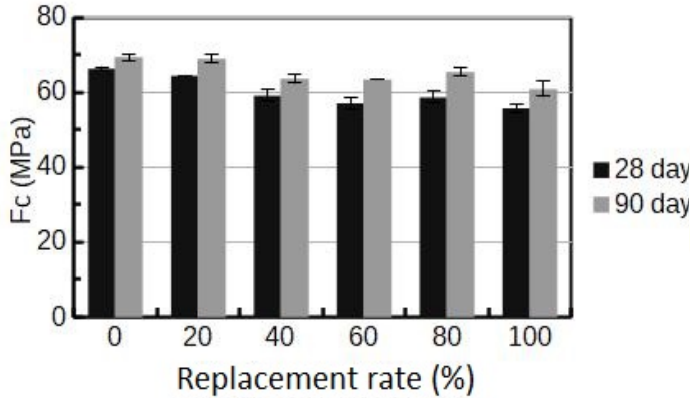


Fig. 2: Compressive strength for different replacement rates

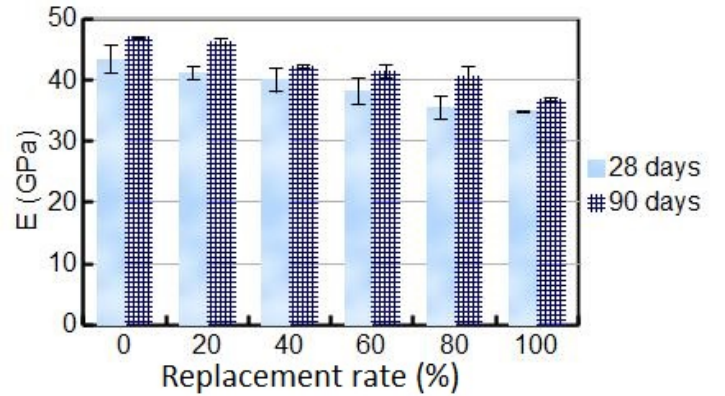


Fig. 3: Elastic modulus for different replacement rates

First, as shown in Fig.2, the compressive strength decreases for increasing replacement rates of natural aggregates by the recycled ones. According to the results, the total replacement of the NA par RCA reduces the compressive strength up to respectively 16% and 12% at 28 and 90 days. This reduction of the compressive strength is quite consistent with other reports in the literature [1, 19] and may be explained by the poor mechanical properties of the attached mortar in recycled aggregates [2]. In addition, since the recycled aggregates are porous materials, they influence the porosity of the recycled concretes and consequently the compressive strength of the formulas. Moreover, the angular shape of the recycled aggregates can also explain this loss in the compressive strength since this aspect disables optimum packing of aggregates and consequently induces large amount of voids in the concretes [20]. However, results presented in Fig.2 show that, up to the replacement rate of 20%, the compressive strength does not exhibit significant variation. This aspect is probably due to the fact that, the 20% of volume replacement rate corresponds to a small mass substitution rate of NA by RCA and the latter is insufficient to induce significant weak zones in the microstructure.

On the other hand, a decrease of 20% and 22% in the elastic moduli is observed for a total replacement of the NA by the RCA (Fig.3) at 28 and 90 days. These results are in accordance with those reported in the literature [19, 21]. The decrease in the elastic modulus of concrete is intrinsically associated to parameters such as the volumetric fractions, the density, and the Young modulus of the recycled aggregates and the interfacial transition zones. These latter are known as porous zones with poor mechanical properties [2]. Consequently, the presence of many interfacial transition zones in RC compared to conventional concretes may explain the difference in the elastic modulus of recycled aggregates concrete. Furthermore, these results may be explained by the aggregates deformations as reported in [20, 22]. Deformation of aggregates are mainly related to their porosity and in a lesser degree to their grading, texture and mineralogical composition.

2.5 Durability properties

This part resumes the results of the durability tests conducted on the specimen under study at 90 days (when the microstructure is relatively stable). Water accessible porosity, rapid chloride diffusion and carbonation tests are carried out on the different formulas, according to the associated standards.

2.5.1 Water accessible porosity

For this test, cylindrical specimens (diameter : 110 mm and 50 mm thick) were submitted to test according to the standard NF P18 – 459 [23]. Two specimens are tested for each replacement rate and the average of the results considered as the corresponding property. The results (Fig.4) show the variation of the water accessible porosity versus the replacement rate. Obviously, the porosity increases with the quantity of the recycled aggregates included in the microstructure. This aspect is first related to the porosity of the recycled aggregates (since these latter exhibit

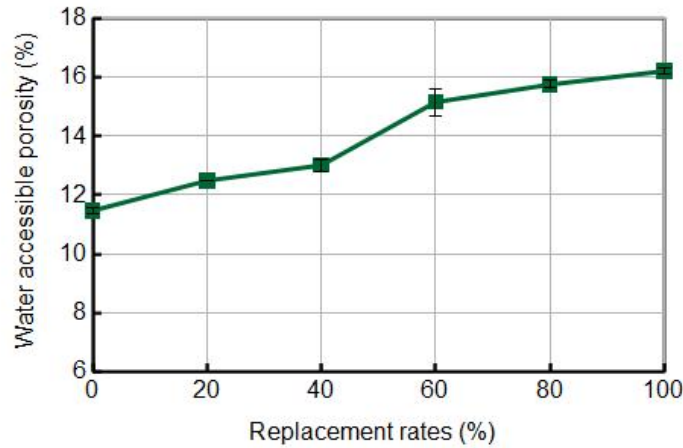


Fig. 4: Water accessible porosity with different replacement rates

high water absorption coefficient (Table1)) and further, due to the loose packing of the RCA in the microstructure of recycled concretes.

2.5.2 Carbonation

Similarly to the case of water accessible porosity, the 50 mm thick cylindrical specimen are submitted to carbonation test according to the slightly modified standard recommendations with 50% of carbon dioxide instead. The results (Fig.5) show the increase of the carbonation depth with quantity of the recycled aggregates in the content. This observation is explained by the porosity of the recycled aggregates associated with the fact that the introduced recycled aggregates are most of the time already carbonated.

2.5.3 Chloride penetration

After 90 days when the microstructure is almost stable, the 50 mm thick specimen are submitted to chloride penetration test according to standard NF EN 12390-11 [24]. The results shown in Fig.6 represent the temporal variation of the chloride cumulative concentration. Obviously, the

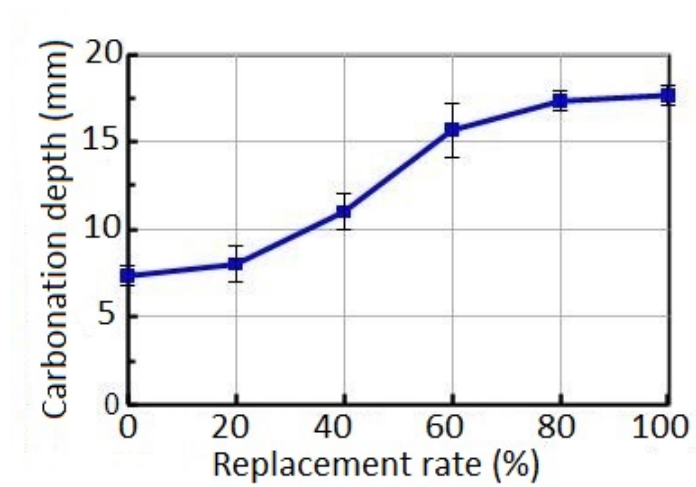


Fig. 5: Carbonation depth with different replacement rates

results show that the quantity of the recycled concrete in the microstructure influences the chloride penetration resistance of the specimen. Consequently, when the concrete content in recycled aggregate increases, the resulting concrete is more porous and the cumulative chloride concentration increases rapidly. As for the chloride diffusion coefficient (Fig.7), it increases with the replacement rate; this aspect is related to the porosity of the obtained recycled concretes.

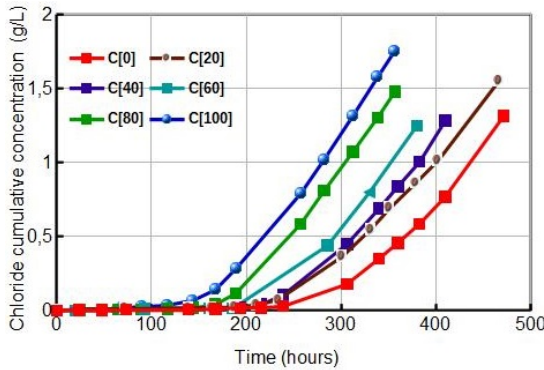


Fig. 6: Chloride cumulative concentration

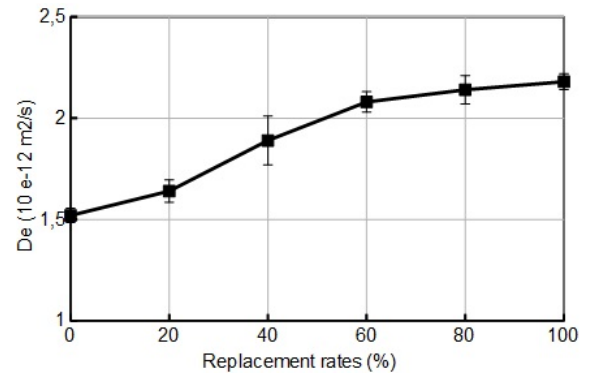


Fig. 7: Evolution of the chloride diffusion coefficient for different formulas of recycled concretes

Furthermore, additional tests are conducted on the new mortar and the reconstructed attached mortar. The latter is made up of the same constituents and mix proportion as the attached mortar in the RCA. The results presented in Table 4 indicate that the new mortar presents a diffusion coefficient greater than that of the reconstructed attached mortar. This result is first related to the content of the reconstructed attached mortar (made up of CEM III cement) and further due to the fact that the reconstructed mortar is not damaged contrary to the real attached mortar in the

RCA. Indeed, as shown in Fig.8, the crushing process induces micro-cracks in the microstructure

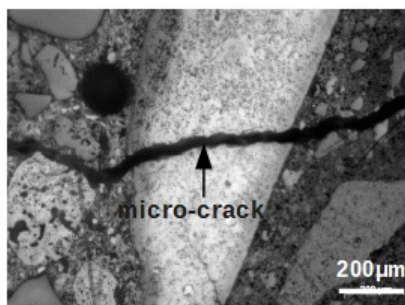


Fig. 8: Typical example of micro-crack observed in the attached mortar

of the attached mortar and consequently facilitates the transport of chloride ions and increases the resulting chloride diffusion coefficient. This effect was also observed in studies conducted by other authors on the diffusion properties of RAC [2, 25, 26]. Our results show a ratio of almost 160 between the diffusion coefficients of respectively the new mortar and the reconstructed attached mortar (Table 4). Nevertheless, it is worth noticing that the real chloride diffusion coefficient of the attached mortar is expected to be greater than that of the reconstructed attached mortar due to the aforementioned effects (presence of the micro-cracks and interface effects).

Phases	New mortar	Reconstructed attached mortar
Diffusion coefficient $\times 10^{-12}(m^2/s)$	2.66	0.0164

TABLE 4: Diffusion coefficient of the new and the reconstructed attached mortar.

3 Investigation on the local mechanical properties

In this part, multi scale indentation technique is used to investigate the mechanical properties of the phases in the microstructure of the RAC. The obtained results are first discussed and further used as input information of the multi scale models developed in the last part. Phases in the cement paste inside the interfacial transition zone are analyzed thanks to statistical indentation technique whereas a direct measurement is used to capture the overall properties of the aggregates and the attached mortar. The indentation depths will be discussed for each considered phase.

3.1 Sample preparation

For indentation tests, samples (20 mm × 20 mm × 10 mm) were cut with a diamond saw and embedded in ethanol solution for 48 hours in order to stop the hydration process of unhydrated clinker. Thereafter, the slices were molded in epoxy resin for 24 hours (when the epoxy gets hardened : see Fig.12). In order to avoid any tilt or wobbling during the test, the faces of the enrobed samples were made parallel by grinding before the polishing. The latter was realized by using dry SiC abrasive papers (1200, 2000 and 4000 grit sizes) followed by the use of alcohol-based diamond suspensions of 3 μ m and 1 μ m grain sizes combined with an alcohol-based lubricant. Similarly to [7], a long polishing at 1 μ m (6 hours) was necessary to get a smooth enough surface in the ITZ (see section 3.5). The studied samples were taken from two formulas, which were chosen according to the presence of the phase of interest (aggregates, ITZ and the old mortar). Therefore, C[60] was chosen because of the presence of the aforementioned zones within the microstructure (Fig.11) whereas C[100] provided sufficient area for large indentation tests (micro indentation) with a reduced disturbance between neighbouring indents.

3.2 Indentation test

Indentation test consists of making contact between a sample (herein sample under study) and an indenter tip of known geometry and mechanical properties. The experimental process is based on two phases : the loading phase (when the indenter is pressed against a specimen with increasing load) and the unloading phase (characterized by a progressive decrease of the load over the sample).The exploitation of the recorded force-displacement curve (P-h) during the two phases helps to derive the mechanical properties of the specimen, which are related to parameters such as the projected contact area between the indenter and the sample surface and the maximum load.

$$M = \frac{\sqrt{\pi}}{2} \frac{S}{\sqrt{A_c}}; \quad H = \frac{P_{max}}{A_c} \quad (1)$$

where $S = \frac{dP}{dh}$ is the measured initial slope of the unloading branch of the P-h curve. Furthermore, A_c , which accounts for the projected contact area of the indenter (on the sample surface), is expressed as function of the indentation depth and depends on the geometry of the indenter tip. Using Oliver and Pharr model [27], the projected area reads : $A_c = 24.5h_c^2$ for perfect Berkovich tip, with h_c accounting for the contact depth (Fig.10). In the case of cylindrical tip, the projected area remains constant since the latter is not related to the contact depth : $A_c = \pi D^2/4$ (D is the diameter of the disc in contact with the sample).

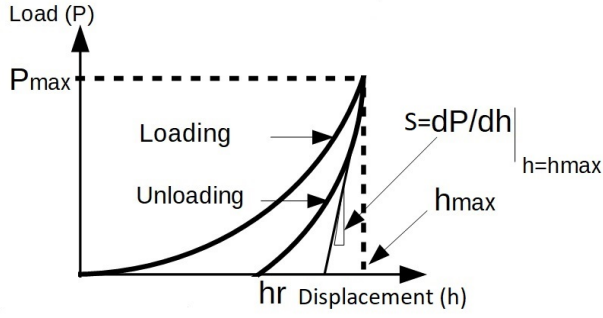


Fig. 9: Load and unloading profile

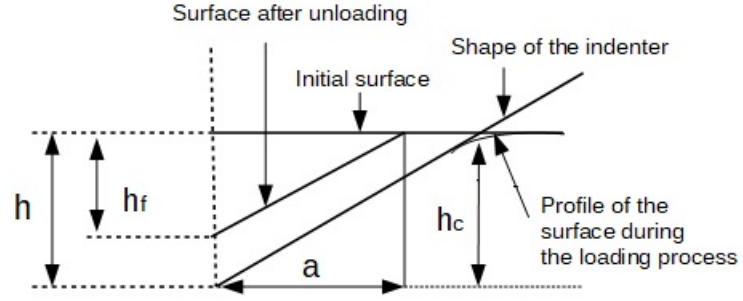


Fig. 10: Geometrical 2D representation of the contact area of Berkovich tip.



Fig. 11: Microstructure of a section of C[60] concrete with phases of interest.

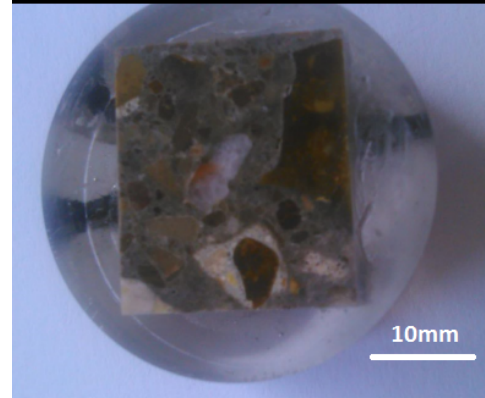


Fig. 12: epoxy enrobed slice.

3.3 Elastic modulus of the aggregates

Indentation of heterogeneous materials requires two different approaches according to the size and the distribution of the phases. The scale separation principle between the indentation depth and the typical size of the heterogeneities governs the measured response. As shown in Fig.13.b, large indentation depth, compared to the heterogeneities length scale, is required to evaluate the effective behavior of a composite whereas indentation length is expected to be small (respecting scale separation principle [28], Fig.13.a) compared to the heterogeneities when investigating individual properties of the phases.

Constantinides et al. [28] established the separation scale relation between the indentation depth and the characteristic size of the heterogeneities inside a composite through continuum indentation analysis :

$$d \ll h_{max} \leq \frac{D}{10} \quad (2)$$

where d is the characteristic length scale of the heterogeneities within a phase, D is the typical

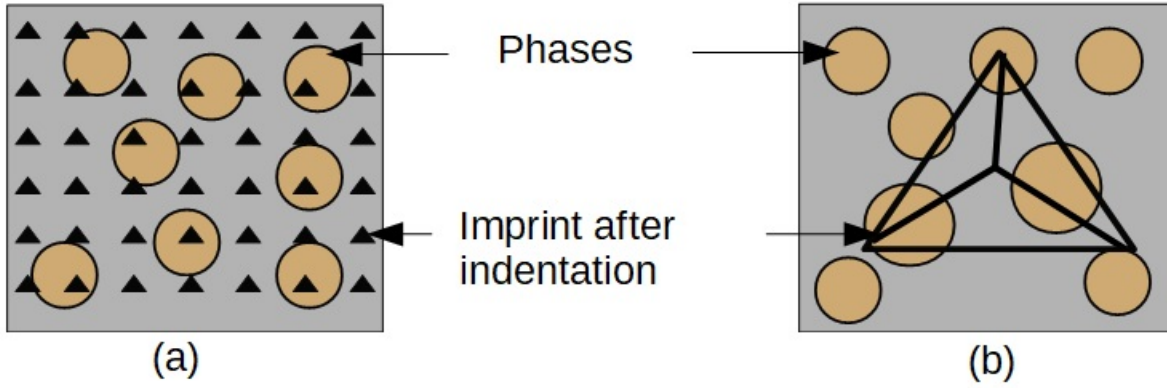


Fig. 13: (a) :scale separation principle ; (b) : Direct measurement principle

size of the phases and h_{max} is the indentation depth that leads to the mechanical properties of each phase individually. Moreover, one deduces from the relation 2, the typical range of the indentation depth accounting for the homogenized response of composite materials ($h_{max} \gg D$). The aggregates under study (calcareous, and siliceous) are viewed as porous materials with relatively small pores sizes ($d \sim 100\text{nm}$). Consequently, one chooses $h_{max} = 1000 \text{ nm}$ as the maximum indentation depth (with a Berkovich tip) on the aggregates (leading to an average maximum force of around 50 mN). Note that this h_{max} value is much lower than the aggregates typical size (20 mm). In addition, the process is conducted with a minimum distance ($30 \times h$) between neighbouring indents in order to avoid any disturbance of the results. The loading and the unloading rate during the indentation test is set to 20 mN/min with a holding time of 1 min. For verification, atomic force microscopy image analysis is done and indicates that, the size of the imprint corresponding to $h_{max} = 1000 \text{ nm}$ is large enough compare to that of the pores (Fig.14,15,16,17). Concerning, the

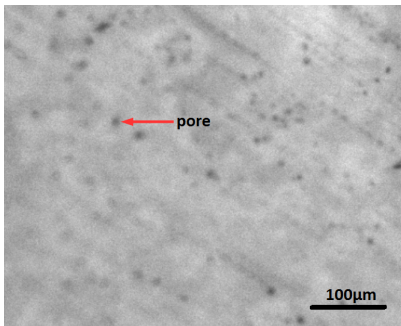


Fig. 14: Optical microscope image of the surface of calcareous aggregate (natural). Typical pore diameter is $d = 100\text{nm}$

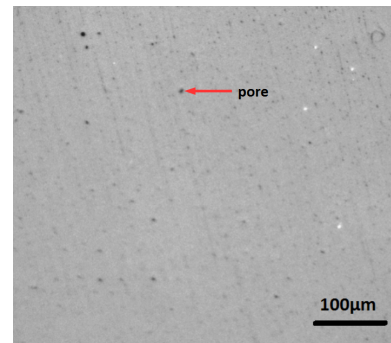


Fig. 15: Optical microscope image of the surface of siliceous aggregate (origin). Typical pore diameter is $d = 100 \text{ nm}$

roughness of the aggregates, Miller [29] criteria, which defines the maximum admissible roughness for each indentation depth, is considered. Consequently, considering the chosen indentation depth ($h_{max} = 1000 \text{ nm}$), the root means square roughness must be less than 200 nm. For the aggregates in study, the obtained roughness after polishing is around 50 nm (in average), satisfying the chosen criteria.

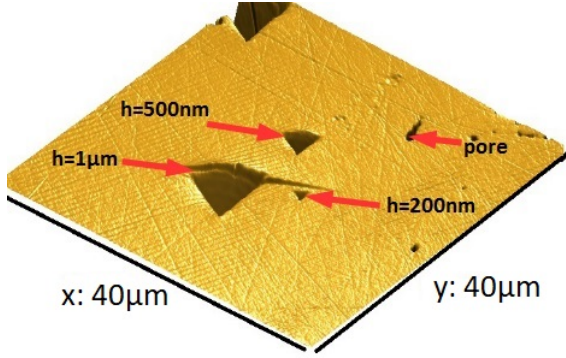


Fig. 16: An atomic resolution scanning probe microscopy image of a residual indent on a calcareous aggregate (natural) for different indentation depths $h = 200, 500, 1000 \text{ nm}$

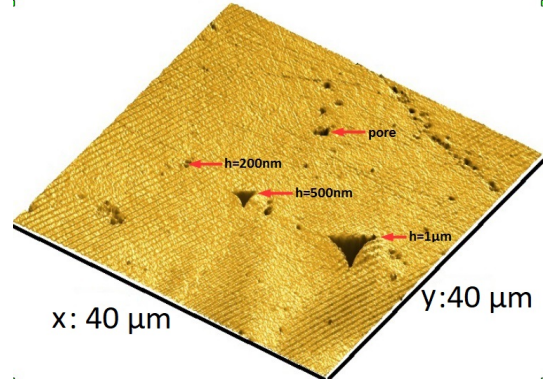


Fig. 17: An atomic resolution scanning probe microscopy image of a residual indent on a siliceous aggregate (from RAC) for different indentation depths $h = 200, 500, 1000 \text{ nm}$

In practice, a reduced number of indentation (typically 50 points) is necessary to stabilize the average indentation modulus (as shown by the standard deviation of the indentation modulus Fig.18,19). In addition, lower indentation depths were tested and confirm that the chosen depth $h_{max} = 1000 \text{ nm}$ is enough to capture the composite indentation modulus of the aggregates : its distribution is narrower and the mean value become independent from the maximum depth. Finally, the found indentation modulus are in a good accordance with results presented in literature for calcareous and siliceous aggregates [30, 31].

3.4 Elastic properties of the attached mortar

The old or the attached mortar is part of the original concrete from which the RCAs are extracted. This phase is usually presented as one of the most damaged zone in the microstructure of RAC [2, 5, 32]. In this approach, the old mortar is viewed as an heterogeneous medium which comprises matrix (cement paste) embedding fine aggregates (sand). The typical size of the latter is around $D=500\mu\text{m}$ (Fig.(21)). For indentation purpose, a microindenter with 6kN of maximum load provided with cylindrical tip (diameter of the contact disc : 1 mm) is used for the indentation

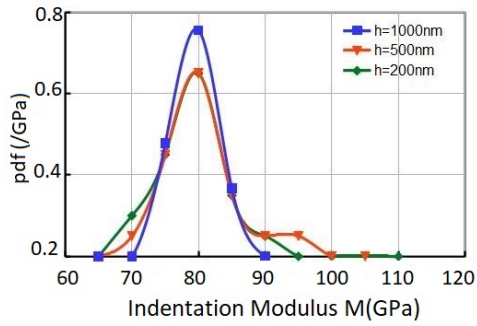


Fig. 18: Distribution (pdf) of the measured indentation modulus for calcareous aggregates

- $h = 1000 \text{ nm}$, $M = 76.66 \pm 2.33 \text{ GPa}$
- $h = 500 \text{ nm}$, $M = 77.64 \pm 5.07 \text{ GPa}$
- $h = 200 \text{ nm}$, $M = 77.49 \pm 4.23 \text{ GPa}$

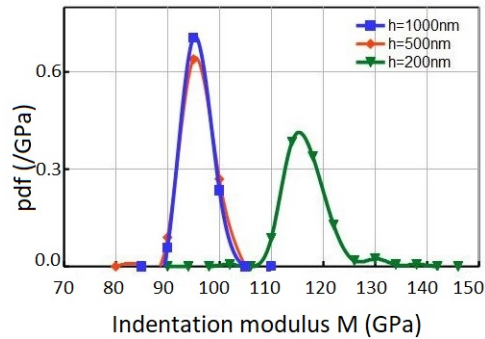


Fig. 19: Distribution (pdf) of the measured indentation modulus for siliceous aggregates

- $h = 1000 \text{ nm}$, $M = 93.50 \pm 2.25 \text{ GPa}$
- $h = 500 \text{ nm}$, $M = 93.06 \pm 2.69 \text{ GPa}$
- $h = 200 \text{ nm}$, $M = 115.63 \pm 6.4 \text{ GPa}$

process on this specimen (Fig.20). The advantage of this kind of tip relies in the constant aspect of the projected area which does not depend on the indentation depth (contrary to Berkovich tip). As for the test parameter, the loading and the unloading rate is set to 5 mm/min with a relaxation time of 1 min. Additionally, a maximum indentation depth of 0.42 mm is chosen for the test since the size of the corresponding imprint is large enough compare to that of the

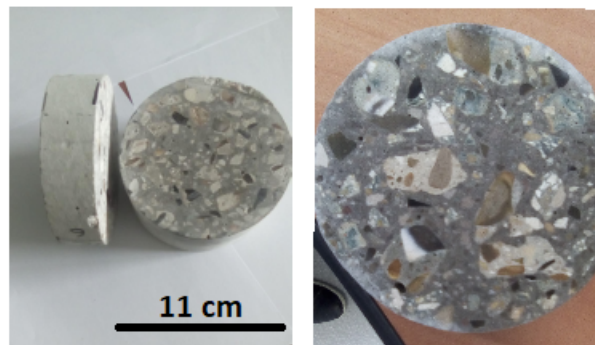


Fig. 20: Typical specimen submitted to micro indentation test

sand grains in this zone (Fig.21). A grid of ten indents is realized on each specimen (Fig.20) and the indentation modulus is obtained by averaging the results of tests conducted on the grid. The choice of the number of indents is guided by the small dispersion of the results. Finally, the average of the realized indentation tests on the two specimens under study leads to the indentation modulus of 16.99 ± 2.85 GPa for the attached mortar. By assuming a Poisson's ratio of 0.2 for the attached mortar, an estimation of the resulting Young modulus is 16.31 ± 2.74 GPa (thanks to the formula $E \sim M \times (1 - \nu^2)$ where M, E, ν represent respectively the indentation modulus, the Young modulus and the Poisson's ratio). Furthermore, considering the Young modulus of the parent concrete (reformulated in laboratory condition) which has been estimated to 35.62 ± 0.47 GPa at 90 days, one notices the difference in elastic modulus of the attached mortar before and after the crushing and confirms the impact of the crushing process on the physical and mechanical properties of the recycled aggregates as reported in the literature [2, 33]. The micro indentation

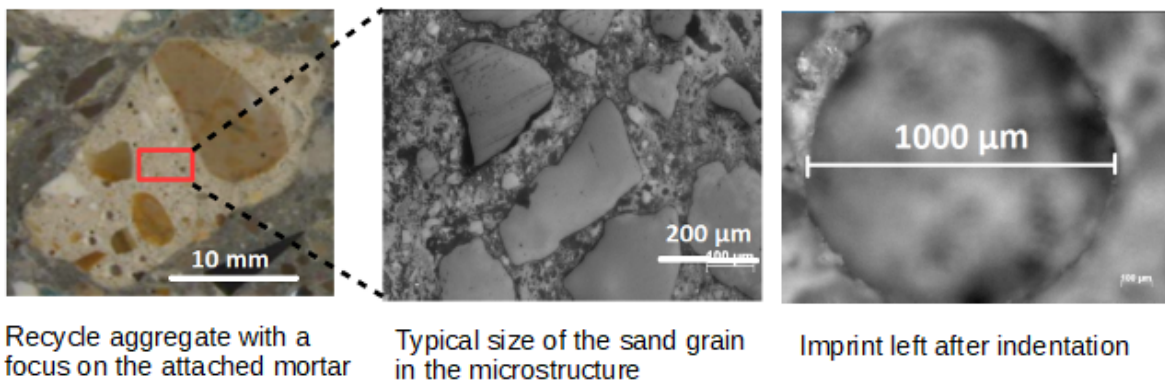


Fig. 21: Microstructure of the attached mortar showing the typical size of the sand grains and the imprint of the largest indentation depth ($h=0.42$ mm)

test gives access to an estimation of the elastic modulus of the old mortar which is difficult to measure due to the configuration of the material under study.

3.5 Elastic properties of the interfacial transition zones (ITZ)

The ITZ plays the role of bridge between the aggregates and the mortar within the microstructure of concretes in general. As described in [2, 34, 35], this phase is made up of highly hydrated cement paste and is consequently more porous than other phases in the microstructure. Topics related to the precise mechanism of formation of this zone are still under studies [36, 37, 38]. As for the typical thickness of this zone, it is reported to be around $50\mu\text{m}$ by Xiao et al.[6]. In this study, for the sake of simplicity and for modeling convenience, one assumed the ITZ as a

cement paste made zone surrounding the aggregates with a constant thickness ($50\mu\text{m}$, Fig.22) and without any gradient of property. In order to measure the homogenized properties of the cement paste, a typical indentation depth of at least $10\mu\text{m}$ should be necessary [39]. However, the size of the imprint corresponding to that indentation depth is too large ($l \simeq 7h = 70\mu\text{m}$) compared to the thickness of the ITZ and the results could be perturbed by the neighbouring phases (aggregates and mortar). Consequently, nanoindentation test (implying small indentation depth) is conducted on the cement paste of the ITZ (from concrete specimen of 28 and 90 days) in order to investigate the mechanical properties of the hydrate phases.

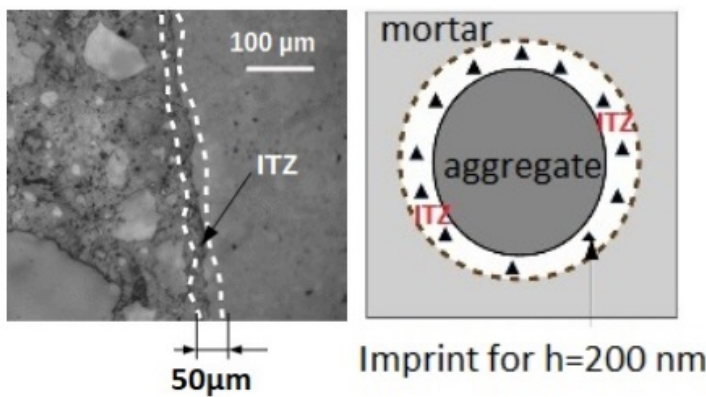


Fig. 22: Delimitation of the interfacial transition zone

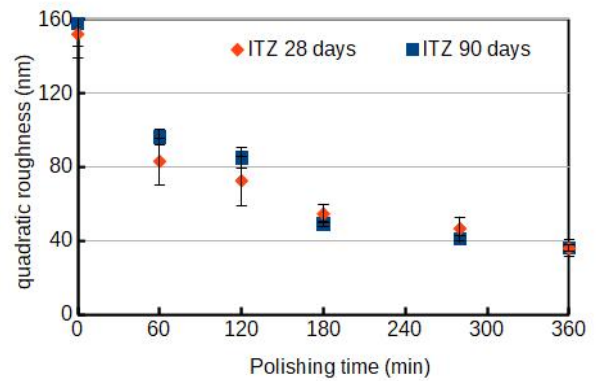


Fig. 23: Evolution of the roughness of the ITZ at 28 and 90 days (during the last time of the polishing process)

The typical range covered by the nanoindentation test is between 6 nm and $2\mu\text{m}$ [7, 28]. This range covers the characteristic length of the encountered phases in the cement paste at nanoscale. Furthermore, considering Constantinides rule [28] (equation 2), the corresponding indentation depth is set to $h_{max} = 200$ nm similarly to nanoindentation tests conducted on cement paste by Vandamme et al.[7]. The expected phases are : LD CSH, HD CSH, UHD CSH, and unhydrated cement. Statistical grid indentation technique is used to extract the mechanical properties of the aforementioned phases similarly to [7]. Since significant contrast is not expected between HD CSH and UHD CSH phases, we associated these two phases in one denoted HD(UHD) CSH. Before the test, the roughness at the surface of the specimen under study are reduced thanks to specific polishing process described in [7, 29]. The typical roughness obtained at the surface of the specimen is around 40 nm in average (Fig.23) fulfilling Miller criteria [29]. Finally, the specimen of 28 and 90 days are submitted to tests and the properties of the phases in the ITZ found at different ages

through deconvolution technique [7, 40, 41, 42]

3.5.1 Results and discussion

Given the multiphase nature of the cement paste within the ITZ, a large array of nanoindentation test is carried out and the results are analyzed statistically. In the process, each indentation point is considered as an independent event for which the corresponding mechanical property is viewed as random variable. Therefore, grids of typically 400 points are analyzed and the results carried out thanks to deconvolution technique. Indeed, the latter consists in fitting the experimental cumulative distribution functions (of indentation modulus and hardness both), by a sum of n theoretical Gaussian distributions. A detailed description of this technique is presented in [7, 40].

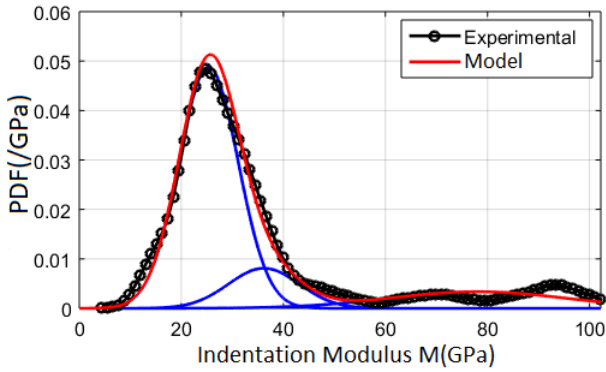


Fig. 24: Probability Density Function (PDF) of the indentation modulus (curves represented in blue are for individual phases)

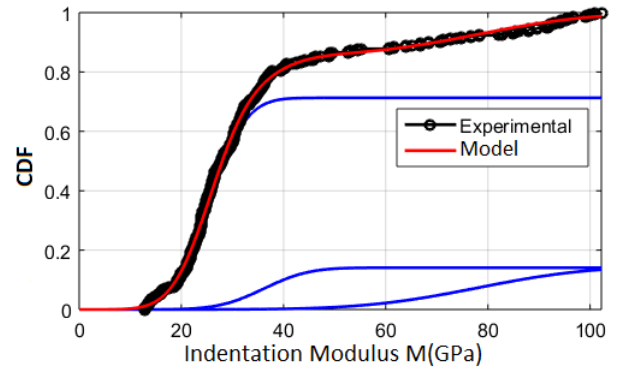


Fig. 25: Cumulative Distribution Function (CDF) of the indentation modulus (curves represented in blue are for individual phases)

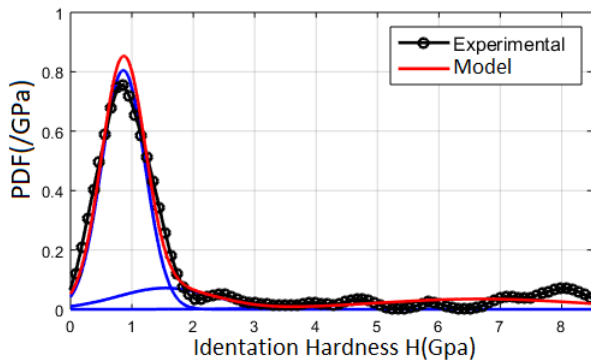


Fig. 26: Probability Density Function (PDF) of the indentation hardness (curves represented in blue are for individual phases)

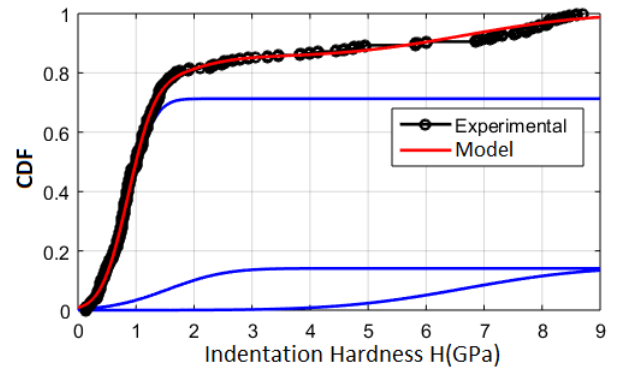


Fig. 27: Cumulative Distribution Function (CDF) of the indentation hardness (curves represented in blue are for individual phases)

After the deconvolution, one gets access to the mechanical properties of each phases (herein

indentation modulus and hardness) with their volume fractions and attributed standard deviations as resumed in Fig.24,25,26,27 and Table 5.

- Phase 1 : this phase is the less rigid among all the identified phases. Compared to data available in the literature, it can be assimilated to low density hydrates phase (LD CSH). The latter is reported in [7, 40] with the following mechanical properties ($M= 22.5 \pm 5.0$ GPa ; $H= 0.61 \pm 0.17$ GPa). Additionally, the results indicate that the volume fraction associated to this phase is around 0.63 at 28 days and 0.34 at 90 days. This variation of the volume fraction is probably related to the densification of the hydrate phases transforming the low density hydrates to more densified ones.

- Phase 2 : mechanical properties of this phase are between that of HD CSH ($M= 30.4 \pm 2.09$ GPa ; $H= 0.92 \pm 0.10$ GPa) and UHD CSH ($M= 40,9 \pm 7,7$ GPa ; $H= 1,46 \pm 0,46$ GPa) [7]. In a recent work, Chen et al.[43] described the UHD CSH phase as a nanocomposite phase made with hydrates foam and portlandite crystals. Even though, the nature of this phase is still under discussion in the literature, we assume that, the measured values correspond to the mechanical properties of composite phase (which comprises the two types of hydrates HD and UHD CSH). Consequently, this phase is denoted HD(UHD) CSH with a volume fraction of 0.23 and 0.53 at respectively 28 and 90 days.

Phases	ITZ 28j			ITZ 90 j		
	M(GPa)	H(GPa)	f	M(GPa)	H(GPa)	f
Phase 1 [LD CSH]	25.62±4.59	0.8±0.26	0.63	25.38±5.01	0.68 ±0.27	0.34
Phase 2 [HD (UHD) CSH]	38.03 ±10.36	1.54±0.23	0.23	36.21±5.03	1.25±0.41	0.53
Phase 3 [Clinker]	86.58±18.84	5.33 ±2.63	0.14	91.10±28.15	6.4±2.81	0.13

TABLE 5: Mechanical properties of the hydrate phases identified in the ITZ at 28 and 90 days.

- Phase 3 : this phase represents the most rigid phase identified and corresponds (according

to available data in the literature $M= 93.4 \pm 44.8$ GPa; $H= 6.13 \pm 4.22$ GPa [7]) to unhydrated cement. The latter is also found to represent 14 and 13% at respectively 28 and 90 days.

4 Micromechanical modeling

In this part, we provide a predicting model accounting for the elastic modulus and the chloride diffusion properties of recycled aggregate concretes, based on the available information on the microstructure (collected in sections 2 and 3). For this purpose, the adopted micromechanical approach is based on the multi-scale characterization of heterogeneous materials (case of cementitious materials). Therefore, a Representative Elementary Volume (REV) is defined and a simplified description of the microstructure is proposed in Fig.28. Finally, the homogenized elastic modulus and the chloride diffusion coefficient are estimated and the results compared to experimental data for discussion.

4.1 Simplified representation of the microstructure

The representation associated to the recycled concrete microstructure comprises at the first scale, the mortar and the different aggregates. For the sake of simplicity and for modeling convenience, all the aggregates are considered as spherical inclusions surrounded by uniform layers of $50\mu\text{m}$ [6] thick representing the ITZs. The choice of this configuration is based on previous results on complex configurations representing the recycled aggregates [44]. These results indicate that, due to the relatively weak contrast between the involved phases, the impact of the distribution of phases within the recycled aggregate is of rather minor importance. Furthermore, the typical ratio of size between the aggregates and the ITZs thickness is set to $e/R \sim 1/100$ where e accounts for the thickness of the interphase and R represents the radius of the spherical inclusion (section 2) . In the same frame, we assume a perfect bonding between the attached mortar and the old aggregates and the detailed description of the microstructure in study is assumed to be made up of three scales as presented in the Fig.28. Moreover, the mechanical properties of phases described in the different scales are extracted from indentation and macroscopic tests.

- Scale I : ($10^{-2}\text{m} \sim 10^{-1}\text{m}$)

This level concerns the first step in the multi scale description of the microstructure of RAC. The latter is assumed to be made up of natural and recycled aggregates (represented respectively by homogeneous and composite inclusions) embedded in homogeneous matrix (herein the mortar which mechanical properties are obtained through macroscopic tests). Moreover, for the sake of

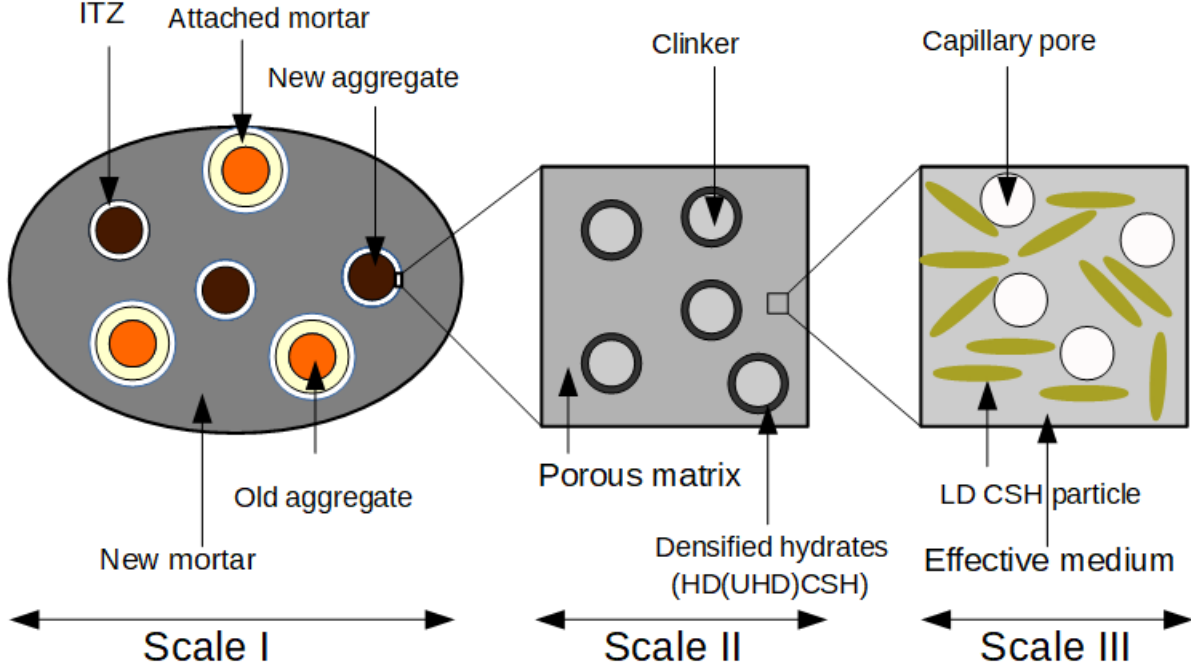


Fig. 28: Simplified representation of the microstructure of RAC

simplicity, one considers the same type of interfacial transition zones around all the aggregates and Mori-Tanaka scheme is used to estimate the effective elastic properties of the RAC at this level. Therefore, considering the REV at scale I (Fig.28), made up of N morphological representative patterns (MRP) [45], the effective stiffness tensor reads :

$$\mathbb{C}^{eff} = \left(\sum_p f_p \mathbb{B}_p \right) : \left(\sum_p f_p \mathbb{A}_p \right)^{-1} \quad (3)$$

where f_p accounts for the volume fraction of the morphological representative pattern 'p' and \mathbb{A}_p and \mathbb{B}_p are fourth order tensors obtained thanks to the Eshelby problem with \mathbf{E}^∞ as the imposed macroscopic strain at infinity. Consequently, \mathbb{A}_p and \mathbb{B}_p satisfy the relations :

$$\langle \boldsymbol{\varepsilon} \rangle_p = \mathbb{A}_p : \mathbf{E}^\infty \quad ; \quad \langle \boldsymbol{\sigma} \rangle_p = \mathbb{B}_p : \mathbf{E}^\infty \quad (4)$$

- Scale II ($10^{-6}\text{m} \sim 10^{-4}\text{m}$)

This scale refers to the cement paste matrix inside the ITZ as shown in Fig.28. The ITZ is assumed to be made up of low density hydrates foam embedding spherical composite inclusions which consists of unhydrated clinker surrounded by high density hydrates. Due to the matrix-inclusion aspect of the microstructure at this specific level, Mori-Tanaka estimate is used to derive **the** homogeneous elastic properties of the ITZ. The effective stiffness tensor of the REV at this

scale is derived according to the equation 3.

- Scale III ($10^{-7}\text{m} \sim 10^{-6}\text{m}$)

In this step, the low density hydrates foam of scale II is regarded as porous media made up of low density hydrates (represented as needle-shape phase exhibiting isotropically distributed orientations [46]) and capillary pores considered as spherical inclusions. Furthermore, as suggested in [47, 48, 49] one considers the hypothesis of a ratio 3/2 between the porosity of the ITZ and that of the neighbouring cement paste. Consequently, by using Powers model [50] one writes :

$$f_{cp}^{ITZ} = \frac{3(e/c - 0.36\alpha)}{2(e/c + 0.32)} \quad (5)$$

Considering the mutual interaction of the considered phases (as in polycrystal), the use the self-consistent scheme is appropriate for the effective stiffness tensor of the REV at this specific scale. Therefore one writes :

$$\mathbf{C}^{eff} = \left[f_{hyd} \mathbf{C}_{hyd} : \int_0^{2\pi} \int_0^\pi \left(\mathbf{I} + \mathbf{P}_{hyd}(\theta, \varphi) : (\mathbf{C}_{hyd} - \mathbf{C}^{eff}) \right)^{-1} \frac{\sin\theta d\theta d\varphi}{4\pi} \right] : \left[f_{cp} \left(\mathbf{I} - \mathbf{P}_{cp} : \mathbf{C}^{eff} \right)^{-1} + f_{hyd} \int_0^{2\pi} \int_0^\pi \left(\mathbf{I} + \mathbf{P}_{hyd}(\theta, \varphi) : (\mathbf{C}_{hyd} - \mathbf{C}^{eff}) \right)^{-1} \frac{\sin\theta d\theta d\varphi}{4\pi} \right]^{-1} \quad (6)$$

where f_{hyd} is the volume of the low density hydrates considered at scale III (Fig.28); \mathbf{C}_{hyd} accounts for the fourth order stiffness tensor of LD CSH (Table 5) and $\mathbf{P}_{cp}, \mathbf{P}_{hyd}$ are Hill tensors of respectively the spherical capillary pores and the needle shape low density hydrates expressed in [51].

The elastic properties of the ITZ are obtained considering the multi scale behavior of the phases present in the microstructure. Furthermore, in order to evaluate the efficiency of the approach, first, additional experiments are performed on a sample of pure cement paste. Secondly, nanoindentation results are combined with parameters such as the w/c ratio and the degree of hydration (obtained through thermogravimetric analysis TGA [52]) and used as input parameter for the multiscale model. Results presented in Table 6, show that the model provides a good estimate of the elastic modulus of the cement paste. Based on these results, the predicted elastic modulus of the ITZ can be considered as reliable results concerning the mechanical properties of the ITZ.

Phases	Age (days)	α	f_{cp}	E(GPa) Model	E(GPa) Macroscopic test
Cement paste	28	0.85	0.15	20.57	21.98±1.56
	90	0.94	0.11	24.01	22.54 ±1.4
ITZ	28	-	0.22	16.08	-
	90	-	0.16	19.95	-

TABLE 6: Elastic modulus of the cement paste and the ITZ (α is the degree of hydration of the cement paste and f_{cp} accounts for the volume fraction of the capillary pores).

4.2 Homogenized properties of the REV

Considering the described microstructure associated to the REV of RAC (Fig.28 : scale I), the effective elastic properties are deduced from the solution of the following problem posed on the representative volume element :

$$\left\{ \begin{array}{ll} \mathbf{div} \boldsymbol{\sigma}(\mathbf{x}) = 0 & (V) \quad (a) \\ \boldsymbol{\sigma}(\mathbf{x}) = \mathbf{C}(\mathbf{x}) : \boldsymbol{\varepsilon}(\mathbf{x}) & (V) \quad (b) \\ \boldsymbol{\varepsilon} = \frac{1}{2}(\mathbf{grad} \boldsymbol{\xi} + {}^t \mathbf{grad} \boldsymbol{\xi}) & (V) \quad (c) \\ \boldsymbol{\xi}(\mathbf{x}) = \mathbf{E} \cdot \mathbf{x} & (\partial V) \quad (d) \end{array} \right. \quad (7)$$

where (7.a) stands for the equilibrium equation at the microscopic scale ($\boldsymbol{\sigma}(\mathbf{x})$ is the stress field), (7.b) accounts for the linear elastic behavior of the phases (\mathbf{C} is the fourth order rigidity tensor) and $\boldsymbol{\varepsilon}$ is the strain field. The latter is related to the displacement $\boldsymbol{\xi}(\mathbf{x})$ field by the relation expressed in the (7.c). Finally, the homogeneous macroscopic strain \mathbf{E} imposed at the boundary of the REV is expressed in (7.d). The latter implies the average rule $\langle \boldsymbol{\varepsilon} \rangle_V = \mathbf{E}$. Considering the relation 3, the effective stiffness tensor of the REV is rewritten in the form :

$$\mathbf{C} = \left((1-f)\mathbf{C}_m + f(1-\lambda)\mathbf{B}_{GN} + f\lambda\mathbf{B}_{GR} \right) : \left((1-f)\mathbf{I} + f(1-\lambda)\mathbf{A}_{GN} + f\lambda\mathbf{A}_{GR} \right)^{-1}$$

$\mathbb{B}_{GN}, \mathbb{B}_{GR}$ are related respectively to the natural aggregates and the recycled aggregates (deduced from the generalized Eshelby problem [53]); \mathbb{C}_m is the stiffness tensor of the mortar. As regards parameters λ and f , they account for the volume fractions of respectively the recycled and natural aggregates.

4.3 Input information of the model

Table 7 summarizes the necessary data concerning the properties of the phases in the microstructure. The elastic modulus of the new mortar at 28 and 90 days are obtained through macroscopic tests. As regards the elastic properties of the attached mortar, the obtained results come from micro indentation test presented in the section 3 of the work. Furthermore, the average of the

Phases	Elastic modulus (GPa)	Poisson ratio [30, 31]
New Mortar (28 days)	31.7	0.2
ITZ (28 days)	16.08	0.23
New Mortar (90 days)	36	0.2
ITZ (90 days)	19.95	0.23
Attached mortar	16.31	0.2
Old Aggregate(siliceous)	92.9	0.08
New Aggregate(Calcareous)	68.81	0.32

TABLE 7: Input information concerning the mechanical properties of phases in the microstructure

volume fraction of the attached mortar (within the recycled aggregate) is found experimentally using the water absorption coefficients of respectively the recycled aggregates, the old aggregates and the recycled sand. Indeed, the latter is supposed to represent the attached mortar. Considering the aforementioned hypothesis, one writes the volumetric relationship between different parts in

the recycled aggregate (with φ accounting for the volume fraction of the 'old natural' aggregate inside the recycled aggregate).

$$w_{recy.aggreg.} = \varphi \times w_{aggreg} + (1 - \varphi) \times w_{old\ mortar} \quad (8)$$

Considering the absorption coefficients of the listed phases (Table 1)

$$w_{recy.aggreg.} = 5.3\%, w_{aggreg} = 1.7\%, w_{old\ mortar} = 9.5 - 11\% \quad (9)$$

one finds :

$$0.53 \leq \varphi \leq 0.61 \quad (10)$$

Therefore, the volume fraction of the attached mortar is found to be around 39 and 47% and is in good accordance with data available in the literature ([3, 54, 55]).

4.3.1 Results and discussion

We compute the effective Young modulus with respect to the replacement rate of natural aggregates by the recycled ones. The properties attributed to each phase is extracted from the available information on the microstructure and resumed in the above paragraphs. Fig.29 shows the compa-

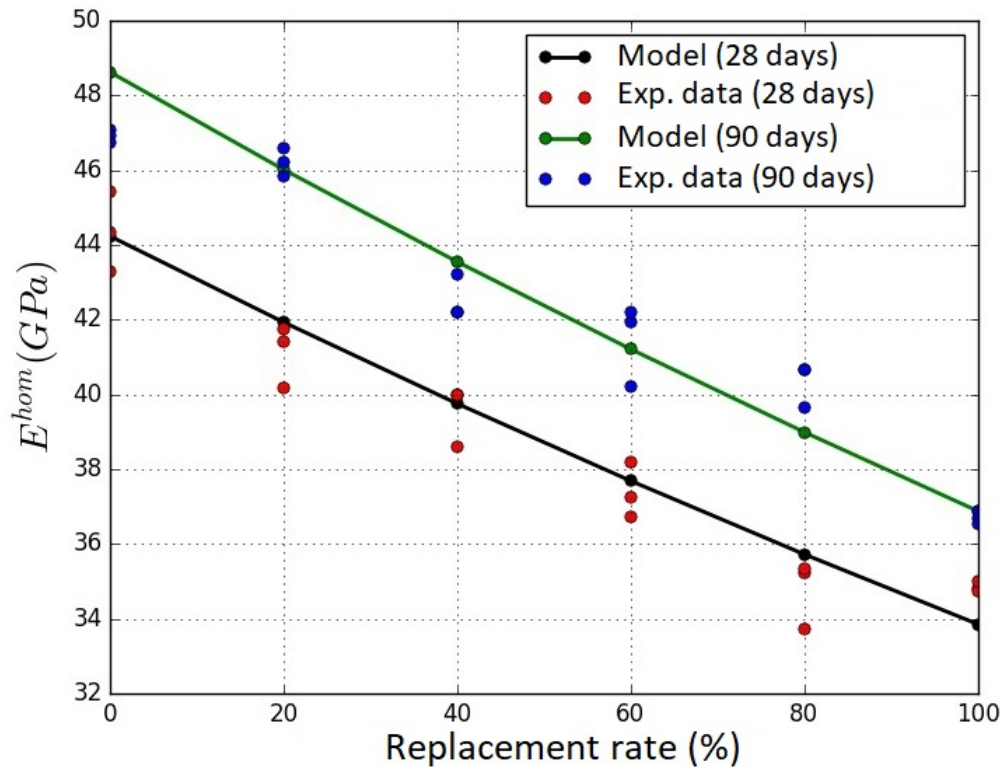


Fig. 29: Evolution of the effective young modulus of concrete with different replacement rates at 28 and 90 days.

parison of the results between the model and the experimental data. Obviously, the predictions of the established models are in the general trend of the experimental results for different replacement rate of NA by RCA. Indeed, the decreasing behavior of the effective elastic modulus (for increasing content of RCA) is probably due to the degraded properties of the old mortar associated to the high number of interfacial transition zones (ITZ). This aspect is also shown in the modeling thanks to the contrast between phases in the composite inclusions representing the recycled aggregates. Consequently, the increase of the volume fraction of the latter inclusions affects the effective elastic modulus of the REV and confirms experimental observations.

On the other hand, the time dependency of the elastic modulus is also predicted by the model at 28 and 90 days. Although macroscopic tests on the mortar (at 28 and 90 days) are directly used as input information in the model, the latter expresses a clear difference between the elastic modulus of the recycled concretes at 28 and 90 days. This particular aspect demonstrates the impact of an evolving elastic properties of individual phases (herein the new mortar) on the overall behavior of the REV as predicted by the model and confirmed by the experimental data.

5 Effective chloride diffusion properties

In this part, the effective chloride diffusion coefficient of the REV (Fig.28) is computed thanks to a multi scale approach. Macroscopic tests are first conducted on the different concretes and the new mortar similarly to the elastic part. As regard the diffusion properties of the attached mortar and the ITZ, they are approximated through optimization process. The typical representation of the microstructure is identical to that presented in Fig.28 with the new and old aggregates herein considered as no diffusive medium ($D = 0$). Only the scale I is considered in the homogenization process. Mori-Tanaka scheme is also used to derive the homogenized diffusion properties of the RVE [56]. The problem posed on the REV is written in the form :

$$\left\{ \begin{array}{ll} \text{div}j(x) = & 0 & (V) & (a) \\ j(x) = & -\mathbf{D}(\mathbf{x}) \cdot \text{grad}\rho(x) & (V) & (b) \\ \rho(x) = & H \cdot x & (\partial V) & (c) \end{array} \right. \quad (11)$$

where relations (a), (b) and (c) are respectively related to the mass balance equation, the Fick law and the uniform density gradient boundary condition (similarly to elasticity) [56] with $\rho, j, H, \mathbf{D}(\mathbf{x})$ accounting for respectively the solute concentration, the diffusion flux, the macro-

scopic concentration gradient and the diffusion tensor. For the sake of simplicity, one denotes $\mathbf{D}_2, \mathbf{D}_{ITZ}$, the diffusion tensor of respectively the attached or old mortar and the ITZ; all assumed as isotropic. The effective diffusion tensor is proportional to the second order unit tensor since the medium is considered as an isotropic material. Thus one writes

$$\mathbf{D}^{hom} = \left(\sum_p f_p \mathbf{B}_p \right) \cdot \left(\sum_p f_p \mathbf{A}_p \right)^{-1} = D^{hom} \mathbf{1} \quad (12)$$

with

$$\langle \text{grad}\rho(x) \rangle_p = \mathbf{A}_p \cdot H^\infty \quad ; \quad \langle j \rangle_p = -\mathbf{B}_p \cdot H^\infty \quad (13)$$

where H^∞ is the imposed macroscopic gradient at infinity (in the generalized Eshelby problem in diffusion) [56] and $\mathbf{1}$ is the second order unit tensor. In the particular case of coated inclusions, the expressions of the concentration tensors are computed thanks to the approaches developed in [57, 58].

5.1 Input information

The input data for this part concerns the chloride diffusion coefficient of the new mortar as resumed in table 4. Additionally, chloride penetration test carried out on a reconstructed attached mortar is considered for further analysis (Table.4). An optimized algorithm based on a least square method is performed in order to identify the chloride diffusion coefficient of the attached mortar and the ITZ.

5.2 Results and discussion

As shown in Fig.30, the Mori-Tanaka based model predicts with an acceptable accuracy, the increase of the chloride diffusion coefficient for different replacement rates. The best fit of the experimental results is obtained for $D_2 = 4.43 \times 10^{-12} m^2/s, D_{ITZ} = 3.9 \times 10^{-11} m^2/s$. **This results** confirm the fact that the interfacial transition zone is probably the most diffusive phase inside the microstructure of RAC. This particular property is surely due to the important porosity of the ITZ as reported in the literature [2, 47]. Moreover, the attached mortar exhibits higher chloride diffusion coefficient compare to the reconstructed mortar. This aspect is probably related to the presence of connected microcracks in the microstructure (induced by the crushing process). Indeed, the microcracks play the role of facilitating the transport of the chloride agent throughout the microstructure and consequently increase the chloride diffusion coefficient of this phase.

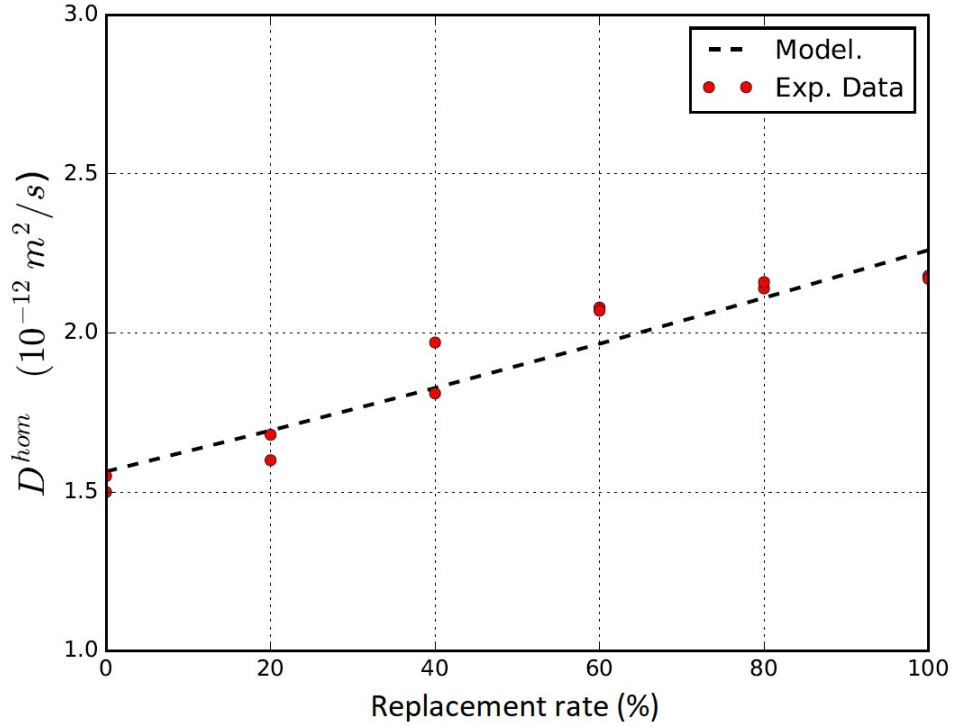


Fig. 30: Diffusion coefficient of RAC with different replacement rates (Obtained results for $D_2 = 4.43 \times 10^{-12} m^2/s, D_{ITZ} = 3.9 \times 10^{-11} m^2/s$).

6 Conclusion

In this work, the mechanical and the chloride diffusion properties of recycled aggregate concretes are investigated at different scales. First, the impact of the recycled aggregates on the RCA is quantified through macroscopic tests. Therefore, the total replacement of natural aggregates by recycled one is found to reduce the compressive strength and the elastic modulus of the concretes up to respectively 12 and 20% (at 90 days) compare to concretes without recycled aggregates. As for the chloride diffusion coefficient, an increase of around 52% is observed for a total replacement of NA by RCA. In the second part, the indentation test conducted on the individual phases of the microstructure helps to collect their mechanical properties (aggregates, ITZ and the attached mortar) present at different scales investigated. The results are shown to be in good accordance with those presented in the literature. In addition, the indentation test helps to confirm the weak mechanical properties of the attached mortar. Finally, the micromechanical based model accounting for the elastic modulus of the concretes according to the replacement rates gives a reliable prediction when compared to experimental data. The impact of the mechanical properties of the individual phases such as the attached mortar and the interfacial transition zones are well expressed in

the model prediction so as the temporal variation of the elastic modulus (at 28 and 90 days). The chloride diffusion properties is also investigated in this work and the results show that optimization approach is efficient to evaluate parameter such as the diffusion coefficient of the ITZ and that of the attached mortar ; information which is difficult to obtain through experimental setup.

7 Acknowledgment

The authors gratefully thank Pr Jian-Fu Shao, Dr Xie Shouyi from LaMCube laboratory (at Lille), Jérôme Carriat and Florencio Thalardiere (From Cerema IdF) and Jean-Marc Plessier from Navier Laboratory for their helpful collaboration.

8 References

- [1] A. B. Fraj, R. Idir, [Concrete based on recycled aggregates – recycling and environmental analysis: A case study of paris’ region](#), Construction and Building Materials 157 (Supplement C) (2017) 952 – 964. doi:<https://doi.org/10.1016/j.conbuildmat.2017.09.059>.
URL <http://www.sciencedirect.com/science/article/pii/S0950061817318615>
- [2] W. N.Otsuki, S.Miyazato, Influence of recycled aggregate on interfacial transition zone, strength, chloride penetration and carbonatation of concrete, Journal of materials in civil engineering 15 (2003) 443–551.
- [3] M. S. de Juan, P. A. Gutiérrez, [Study on the influence of attached mortar content on the properties of recycled concrete aggregate](#), Construction and Building Materials 23 (2) (2009) 872 – 877. doi:<https://doi.org/10.1016/j.conbuildmat.2008.04.012>.
URL <http://www.sciencedirect.com/science/article/pii/S0950061808001086>
- [4] M. A.K. Padmini, K.Ramamurthy, Influence of parent concrete on the properties of recycled aggregate concrete, Construction and Building Materials 23 (2009) 829–836.
- [5] A. Abbas, G. Fathifazl, O. Isgor, A. Razaqpur, B.Fournier, S.Foo, Durability of recycled aggregate concrete designed with equivalent volume method, Cement Concrete Composite 31 (2009) 555–563.
- [6] J. Xiao, W. Li, Z. Sun, D. A. Lange, S. P. Shah, [Properties of interfacial transition zones in recycled aggregate concrete tested by nanoindentation](#), Cement and Concrete Composites

- 37 (Supplement C) (2013) 276 – 292. doi:<https://doi.org/10.1016/j.cemconcomp.2013.01.006>.
URL <http://www.sciencedirect.com/science/article/pii/S0958946513000085>
- [7] M. Vandamme, F.-J. Ulm, P. Fonollosa, [Nanogranular packing of c–s–h at substoichiometric conditions](#), Cement and Concrete Research 40 (1) (2010) 14 – 26. doi:<https://doi.org/10.1016/j.cemconres.2009.09.017>.
URL <http://www.sciencedirect.com/science/article/pii/S0008884609002701>
- [8] C. Thomas, J. Setién, J. Polanco, P. Alaejos, M. S. de Juan, [Durability of recycled aggregate concrete](#), Construction and Building Materials 40 (Supplement C) (2013) 1054 – 1065, special Section on Recycling Wastes for Use as Construction Materials. doi:<https://doi.org/10.1016/j.conbuildmat.2012.11.106>.
URL <http://www.sciencedirect.com/science/article/pii/S0950061812009427>
- [9] A. U. Nilsen, P. J. Monteiro, [Concrete: A three phase material](#), Cement and Concrete Research 23 (1) (1993) 147 – 151. doi:[https://doi.org/10.1016/0008-8846\(93\)90145-Y](https://doi.org/10.1016/0008-8846(93)90145-Y).
URL <http://www.sciencedirect.com/science/article/pii/000888469390145Y>
- [10] H. Ghorbanbeigi, W. Shen, I. Yurtdas, J.-F. Shao, [A micromechanics-based model for concrete materials subjected to carbonation](#), International Journal for Numerical and Analytical Methods in Geomechanics 40 (8) (2016) 1203–1218. arXiv:<https://onlinelibrary.wiley.com/doi/pdf/10.1002/nag.2479>, doi:[10.1002/nag.2479](https://doi.org/10.1002/nag.2479).
URL <https://onlinelibrary.wiley.com/doi/abs/10.1002/nag.2479>
- [11] W. Q. Shen, J. F. Shao, D. Kondo, [A micromechanical study of drying and carbonation effects in cement-based materials](#), Continuum Mechanics and Thermodynamics 27 (1) (2015) 49–61. doi:[10.1007/s00161-013-0327-4](https://doi.org/10.1007/s00161-013-0327-4).
URL <https://doi.org/10.1007/s00161-013-0327-4>
- [12] S. J.F. Ungar, [Multiscale Modeling of Concrete. From Mesoscale to Macroscale](#), Springer New York, 2011, pp. 341–393.
URL <https://doi.org/10.1007/s11831-011-9063-8>
- [13] [EN 933-11 : Tests for geometrical properties of aggregates – Part 11 : Classification test for the constituents of coarse recycled aggregate](#), European Standard, 2009.

- [14] EN 1097-6 : Tests for mechanical and physical properties of aggregates – Part 6 : Determination of particle density and water absorption, European Standard, 2014.
- [15] EN 1097-2, Tests for mechanical and physical properties of aggregates – Part 2 : Methods for determination of resistance to fragmentation, European Standard, 2010.
- [16] EN 12350-2 :Testing fresh concrete-Part 2 : Slump test, European Standard, 2009.
- [17] EN 12390-3 : Testing hardened concrete – Part 3 : Compressive strength of test specimens, European Standard, 2012.
- [18] EN 12390-13 : Testing hardened concrete – Part 13 : Elastic modulus of test specimens, European Standard, 2012.
- [19] A. M. Wagih, H. Z. El-Karmoty, M. Ebid, S. H. Okba, [Recycled construction and demolition concrete waste as aggregate for structural concrete](#), HBRC Journal 9 (3) (2013) 193 – 200. doi:<https://doi.org/10.1016/j.hbrcj.2013.08.007>.
URL <http://www.sciencedirect.com/science/article/pii/S1687404813000588>
- [20] P. Agamuthu, [Challenges in sustainable management of construction and demolition waste](#), Waste Management & Research 26 (6) (2008) 491–492, pMID : 19039063. arXiv:<https://doi.org/10.1177/0734242X08100096>, doi:10.1177/0734242X08100096.
URL <https://doi.org/10.1177/0734242X08100096>
- [21] R. V. Silva, J. de Brito, R. K. Dhir, [Establishing a relationship between modulus of elasticity and compressive strength of recycled aggregate concrete](#), Journal of Cleaner Production 112 (Part 4) (2016) 2171 – 2186. doi:<https://doi.org/10.1016/j.jclepro.2015.10.064>.
URL <http://www.sciencedirect.com/science/article/pii/S0959652615015358>
- [22] P. K. Mehta, Concrete : Structure, properties and materials.
- [23] NF P18-459 : Testing hardened concrete – Testing porosity and density, French Standard, 2010.
- [24] EN 12390-11 : Testing hardened concrete- Determination of the chloride resistance of concrete ; unidirectional diffusion, European Standard 2015.

- [25] F. Olorunsogo, N. Padayachee, [Performance of recycled aggregate concrete monitored by durability indexes](#), Cement and Concrete Research 32 (2) (2002) 179 – 185. doi:[https://doi.org/10.1016/S0008-8846\(01\)00653-6](https://doi.org/10.1016/S0008-8846(01)00653-6).
URL <http://www.sciencedirect.com/science/article/pii/S0008884601006536>
- [26] J. Xiao, J. Ying, V. W. Y. Tam, I. R. Gilbert, [Test and prediction of chloride diffusion in recycled aggregate concrete](#), Science China Technological Sciences 57 (12) (2014) 2357–2370. doi:[10.1007/s11431-014-5700-4](https://doi.org/10.1007/s11431-014-5700-4).
URL <https://doi.org/10.1007/s11431-014-5700-4>
- [27] W. Oliver, G. Pharr, An improved technique for determining hardness and elastic modulus using load and displacement sensing indentation experiments, Journal of Materials Research 7 (6) (1992) 1564–1583. doi:[10.1557/JMR.1992.1564](https://doi.org/10.1557/JMR.1992.1564).
- [28] G. Constantinides, K. R. Chandran, F.-J. Ulm, K. V. Vliet, [Grid indentation analysis of composite microstructure and mechanics: Principles and validation](#), Materials Science and Engineering : A 430 (1) (2006) 189 – 202. doi:<https://doi.org/10.1016/j.msea.2006.05.125>.
URL <http://www.sciencedirect.com/science/article/pii/S0921509306009294>
- [29] M. Miller, C. Bobko, M. Vandamme, F.-J. Ulm, [Surface roughness criteria for cement paste nanoindentation](#), Cement and Concrete Research 38 (4) (2008) 467 – 476. doi:<https://doi.org/10.1016/j.cemconres.2007.11.014>.
URL <http://www.sciencedirect.com/science/article/pii/S0008884607002955>
- [30] M. Chalhoub, Massifs rocheux : Homogénéisation et classification numériques, 2009, presses de Paritech.
- [31] G. Mavko, T. Mukerji, J. Dvorkin, The rock physics handbook. Tools for seismic analysis in porous media, 2009, cambridge University Press.
- [32] J. J. Thomas, J. J. Biernacki, J. W. Bullard, S. Bishnoi, J. S. Dolado, G. W. Scherer, A. Luttge, [Modeling and simulation of cement hydration kinetics and microstructure development](#), Cement and Concrete Research 41 (12) (2011) 1257 – 1278, conferences Special : Cement Hydration Kinetics and Modeling, Quebec City, 2009 amp ; CONMOD10, Lausanne,

2010. doi:<http://dx.doi.org/10.1016/j.cemconres.2010.10.004>.

URL <http://www.sciencedirect.com/science/article/pii/S0008884610002796>

- [33] A. Abbas, G. Fathifazl, B. Fournier, O. Isgor, R. Zavadil, A. Razaqpur, S. Foo, [Quantification of the residual mortar content in recycled concrete aggregates by image analysis](#), *Materials Characterization* 60 (7) (2009) 716 – 728, 11th Euroseminar on Microscopy Applied to Building Materials (EMABM). doi:<https://doi.org/10.1016/j.matchar.2009.01.010>.
URL <http://www.sciencedirect.com/science/article/pii/S1044580309000254>
- [34] M. Königsberger, B. Pichler, C. Hellmich, [Micromechanics of itz–aggregate interaction in concrete part i: Stress concentration](#), *Journal of the American Ceramic Society* 97 (2) (2014) 535–542. doi:[10.1111/jace.12591](https://doi.org/10.1111/jace.12591).
URL <http://dx.doi.org/10.1111/jace.12591>
- [35] K. L. Scrivener, K. M. Nemati, The percolation of pore space in the cement paste/aggregate interfacial zone of concrete, *Cement and Concrete Research* 26 (1) (1996) 35–40, cited By (since 1996) : 87 Export Date : 1 June 2011 Source : Scopus. doi:[10.1016/0008-8846\(95\)00185-9](https://doi.org/10.1016/0008-8846(95)00185-9).
- [36] B. Barnes, S. Diamond, W. Dolch, [The contact zone between portland cement paste and glass “aggregate” surfaces](#), *Cement and Concrete Research* 8 (2) (1978) 233 – 243. doi:[https://doi.org/10.1016/0008-8846\(78\)90012-1](https://doi.org/10.1016/0008-8846(78)90012-1).
URL <http://www.sciencedirect.com/science/article/pii/0008884678900121>
- [37] Z. Hashin, P. Monteiro, [An inverse method to determine the elastic properties of the interphase between the aggregate and the cement paste](#), *Cement and Concrete Research* 32 (8) (2002) 1291 – 1300. doi:[https://doi.org/10.1016/S0008-8846\(02\)00792-5](https://doi.org/10.1016/S0008-8846(02)00792-5).
URL <http://www.sciencedirect.com/science/article/pii/S0008884602007925>
- [38] R. Zimbelmann, [A contribution to the problem of cement-aggregate bond](#), *Cement and Concrete Research* 15 (5) (1985) 801 – 808. doi:[https://doi.org/10.1016/0008-8846\(85\)90146-2](https://doi.org/10.1016/0008-8846(85)90146-2).
URL <http://www.sciencedirect.com/science/article/pii/0008884685901462>
- [39] S. Liang, Y. Wei, Z. Wu, [Multiscale modeling elastic properties of cement-based materials considering imperfect interface effect](#), *Construction and Building Materials* 154 (Supplement

- C) (2017) 567 – 579. doi:<https://doi.org/10.1016/j.conbuildmat.2017.07.196>.
URL <http://www.sciencedirect.com/science/article/pii/S0950061817315398>
- [40] L. Sorelli, G. Constantinides, F.-J. Ulm, F. Toutlemonde, [The nano-mechanical signature of ultra high performance concrete by statistical nanoindentation techniques](#), Cement and Concrete Research 38 (12) (2008) 1447 – 1456. doi:<https://doi.org/10.1016/j.cemconres.2008.09.002>.
URL <http://www.sciencedirect.com/science/article/pii/S0008884608001567>
- [41] G. Constantinides, F.-J. Ulm, The nanogranular nature of C S H, Journal of Mechanics Physics of Solids 55 (2007) 64–90. doi:[10.1016/j.jmps.2006.06.003](https://doi.org/10.1016/j.jmps.2006.06.003).
- [42] G. Constantinides, Invariant mechanical properties of calcium-silicate-hydrates (c-s-h) in cement-based materials : instrumented nanoindentation and microporomechanical modeling, Ph.D. thesis, massachusettsInstitute of Technology (2006).
- [43] J. J. Chen, L. Sorelli, M. Vandamme, F.-J. Ulm, G. Chanvillard, [A coupled nanoindentation/SEM-EDS study on low water/cement ratio Portland cement paste: Evidence for C-S-H/Ca\(OH\)₂ nanocomposites](#), Journal of the American Ceramic Society 93 (5) (2010) 1484–1493. doi:[10.1111/j.1551-2916.2009.03599.x](https://doi.org/10.1111/j.1551-2916.2009.03599.x).
URL <https://hal.archives-ouvertes.fr/hal-00555495>
- [44] A. Adessina, J.-F. Barthélémy, F. Lavergne, A. Ben Fraj, [Effective elastic properties of materials with inclusions of complex structure](#), International Journal of Engineering Science 119 (2017) 1 – 15. doi:<https://doi.org/10.1016/j.ijengsci.2017.03.015>.
URL <http://www.sciencedirect.com/science/article/pii/S0020722517304809>
- [45] A. Zaoui, [Structural Morphology and Constitutive Behaviour of Microheterogeneous Materials](#), Springer Vienna, Vienna, 1997, pp. 291–347. doi:[10.1007/978-3-7091-2662-2_6](https://doi.org/10.1007/978-3-7091-2662-2_6).
URL http://dx.doi.org/10.1007/978-3-7091-2662-2_6
- [46] B. Pichler, C. Hellmich, Upscaling quasi-brittle strength of cement paste and mortar : A multi-scale engineering mechanics model, Cement and Concrete Research 41 (2011) 467–476.
- [47] B. H. Oh, S. Y. Jang, [Prediction of diffusivity of concrete based on simple analytic equations](#), Cement and Concrete Research 34 (3) (2004) 463 – 480. doi:<https://doi.org/10.1016/j>.

[cemconres.2003.08.026](#).

URL <http://www.sciencedirect.com/science/article/pii/S0008884603003119>

- [48] Y. Gao, G. D. Schutter, G. Ye, Z. Tan, K. Wu, [The itz microstructure, thickness and porosity in blended cementitious composite: Effects of curing age, water to binder ratio and aggregate content](#), Composites Part B : Engineering 60 (2014) 1 – 13. doi:<https://doi.org/10.1016/j.compositesb.2013.12.021>.

URL <http://www.sciencedirect.com/science/article/pii/S1359836813007518>

- [49] R. A. Patel, Q. T. Phung, S. C. Seetharam, J. Perko, D. Jacques, N. Maes, G. D. Schutter, G. Ye, K. V. Breugel, [Diffusivity of saturated ordinary portland cement-based materials: A critical review of experimental and analytical modelling approaches](#), Cement and Concrete Research 90 (2016) 52 – 72. doi:<https://doi.org/10.1016/j.cemconres.2016.09.015>.

URL <http://www.sciencedirect.com/science/article/pii/S0008884615302222>

- [50] T. C. Powers, T. L. Brownyard, [Studies of the physical properties of hardened portland cement paste](#), Journal Proceedings 43 (9). doi:[10.14359/15302](https://doi.org/10.14359/15302).

- [51] B. Pichler, C. Hellmich, J. Eberhardsteiner, [Spherical and acicular representation of hydrates in a micromechanical model for cement paste: prediction of early-age elasticity and strength](#), Acta Mechanica 203 (3) (2008) 137. doi:[10.1007/s00707-008-0007-9](https://doi.org/10.1007/s00707-008-0007-9).

URL <https://doi.org/10.1007/s00707-008-0007-9>

- [52] J. Byfors, [Plain concrete at early ages](#), Ph.D. thesis, these de doctorat. Swedish Cement and Concrete Institute (1980).

- [53] E. Herve, A. Zaoui, [n-layered inclusion-based micromechanical modelling](#), International Journal of Engineering Science 31 (1) (1993) 1 – 10. doi:[http://dx.doi.org/10.1016/0020-7225\(93\)90059-4](http://dx.doi.org/10.1016/0020-7225(93)90059-4).

URL <http://www.sciencedirect.com/science/article/pii/0020722593900594>

- [54] S. Braymand, S. Roux, H. Fares, K. Déodonne, F. Feugeas, [Separation and quantification of attached mortar in recycled concrete aggregates](#), Waste and Biomass Valorization 8 (5) (2017) 1393–1407. doi:[10.1007/s12649-016-9771-2](https://doi.org/10.1007/s12649-016-9771-2).

URL <https://doi.org/10.1007/s12649-016-9771-2>

- [55] M. Etxeberria, E. Vázquez, A. Marí, M. Barra, [Influence of amount of recycled coarse aggregates and production process on properties of recycled aggregate concrete](#), *Cement and Concrete Research* 37 (5) (2007) 735 – 742. doi:<https://doi.org/10.1016/j.cemconres.2007.02.002>.
URL <http://www.sciencedirect.com/science/article/pii/S0008884607000415>
- [56] L. Dormieux, D. Kondo, F. Ulm, *Microporomechanics*, Wiley, 2006.
- [57] S. Caré, E. Hervé, [Application of a n-phase model to the diffusion coefficient of chloride in mortar](#), *Transport in Porous Media* 56 (2) (2004) 119–135. doi:[10.1023/B:TIPM.0000021730.34756.40](https://doi.org/10.1023/B:TIPM.0000021730.34756.40).
URL <https://doi.org/10.1023/B:TIPM.0000021730.34756.40>
- [58] E. Herve, [Thermal and thermoelastic behaviour of multiply coated inclusion-reinforced composites](#), *International Journal of Solids and Structures* 39 (4) (2002) 1041 – 1058. doi:[https://doi.org/10.1016/S0020-7683\(01\)00257-8](https://doi.org/10.1016/S0020-7683(01)00257-8).
URL <http://www.sciencedirect.com/science/article/pii/S0020768301002578>